

New Vanadium Tris(*tert*-butoxy)siloxy Complexes and Their Thermolytic Conversions to Vanadia–Silica Materials

Kyle L. Fuldala and T. Don Tilley*

Department of Chemistry, University of California, Berkeley, Berkeley, California 94720-1460,
and Chemical Sciences Division, Lawrence Berkeley Laboratory, 1 Cyclotron Road,
Berkeley, California 94720

Received October 12, 2001

The V(IV) alkoxysiloxy complexes (tBuO)₃VOSi(O^iBu)₃ (**1**) and (tBuO)₂V[OSi(O^iBu)₃]₂ (**2**) were synthesized via the silanolysis of V(O^iBu)₄ with 1 and 2 equiv of HOSi(O^iBu)₃, respectively. Complexes **1** and **2** are efficient single-source molecular precursors to homogeneous V/Si/O materials via the *thermolytic molecular precursor* method. The thermal transformations of these complexes occurred at low temperatures (≤ 160 °C), via the elimination of isobutene as the major carbon-containing product. Thermolyses of **1** in the solid state and in solution (forming a xerogel in the latter case) yielded V/Si/O materials (**VOSi1_{ss}** and **VOSi1_{xg}**, respectively) with low surface areas (30–40 m² g^{−1}). After calcination at 400 °C in O₂, these materials exhibited powder X-ray diffraction (PXRD) patterns consistent with the presence of V₂O₅. Similar thermolyses of **2** yielded V/Si/O materials (**VOSi2_{ss}** and **VOSi2_{xg}**) that exhibited higher surface areas (up to 170 and 70 m² g^{−1}, respectively) and V₂O₅ crystallite formation after calcination at 400 °C. Comparisons of **VOSi1_{xg}** and **VOSi2_{xg}** with a previously reported V/Si/O xerogel (**VOSi3_{xg}**), generated from the V(V) precursor OV[OSi(O^iBu)₃]₃, revealed interesting differences. Crystalline V₂O₅ was first observed in **VOSi3_{xg}** after calcination at only 300 °C in O₂. Transmission electron microscopy (TEM) and PXRD were used to determine that the average size of the V₂O₅ crystallites in the V/Si/O xerogels, after calcination at a given temperature, increased with increasing silicon content of the precursor and was highest for the V(V) tris(siloxide). The precursors containing vanadium in the lower oxidation state (IV) appear to initially provide more homogeneous V/Si/O materials. Higher Si content for the precursor leads to a greater surface area for the resultant material, but also to earlier phase separation during the calcination process.

Introduction

Atomic-level control over solid-state structures is of fundamental importance for the preparation of new materials with unique properties.¹ To that end, there has been significant research toward the development and understanding of low-temperature routes to new materials. A commonly used low-temperature method for the preparation of oxides is the sol–gel process. This method often involves the hydrolysis and condensation of alkoxide precursors, typically in polar media (such as ROH or H₂O).² Although effective for the synthesis of single-component oxides, traditional sol–gel routes can be problematic for the generation of homogeneous mixed-element oxides due to large differences in the hydrolysis rates of the alkoxide precursors.^{2,3} This can be addressed to some extent by careful modification of

the structure of the precursors (e.g., by varying the steric properties of substituents or by use of chelating ligands). Alternatively, improved homogeneity may result from the prehydrolysis of one precursor prior to the addition of a second.^{2,3} To overcome problems associated with the sol–gel process, the development of alternative low-temperature methods for the synthesis of more complicated heteroelement oxides is desired.

Recent advances toward molecular-level control over the synthesis of materials have included the use of single-source molecular precursors.⁴ Potential advantages to this approach include the efficient incorporation

(1) (a) *Ultrastructure Processing of Advanced Materials*, Uhlmann, D. R., Ulrich, D. R., Eds.; Wiley-Interscience: New York, 1992. (b) *Better Ceramics Through Chemistry VI*; Cheetham, A. K., Brinker, C. J., McCartney, M. L., Sanchez, C., Eds.; Materials Research Society Symposium Proceedings 360; Materials Research Society: Pittsburgh, PA, 1994, and previous volumes. (c) *Inorganic Materials*, Bruce, D. W., O'Hare, D., Eds.; Wiley: New York, 1992. (d) *Ceramic Precursor Technology and Its Applications*; Narula, C. K., Marcel Dekker, Inc.: New York, 1995. (e) Bowes, C. L.; Ozin, G. A. *Adv. Mater.* **1996**, *8*, 13. (f) Stein, A.; Keller, S. W.; Mallouk, T. E. *Science* **1993**, *259*, 1558. (g) Mehrotra, R. C. *J. Non-Cryst. Solids* **1988**, *100*, 1. (h) Amabilino, D. B.; Stoddart, J. F. *Chem. Rev.* **1995**, *95*, 2725.

(2) (a) Brinker, C. J.; Scherer, G. W. *Sol–Gel Science*; Academic Press: Boston, 1990. (b) *Sol–Gel Technology for Thin Films, Fibers, Preforms, Electronics, and Specialty Shapes*; Klein, L. C., Ed.; Noyes: Park Ridge, NJ, 1988. (c) Brinker, C. J. *J. Non-Cryst. Solids* **1988**, *100*, 31. (d) Corriu, R. J. P.; Leclercq, D. *Angew. Chem., Int. Ed. Engl.* **1996**, *35*, 1421. (e) Schmidt, H. J. *Non-Cryst. Solids* **1988**, *100*, 51.

(3) (a) Schubert, U. *J. Chem. Soc., Dalton Trans.* **1996**, 3343. (b) Schubert, U.; Hüsing, N.; Lorenz, A. *Chem. Mater.* **1995**, *7*, 2010.

(4) Selected references on the single-source precursor approach: (a) Cowley, A. H.; Jones, R. A. *Angew. Chem., Int. Ed. Engl.* **1989**, *28*, 1208. (b) Appleby, A. W.; Warren, A. C.; Barron, A. R. *Chem. Mater.* **1992**, *4*, 167. (c) Chaput, F.; Lecomte, A.; Dauger, A.; Boilot, J. P. *Chem. Mater.* **1989**, *1*, 199. (d) Hubert-Pfalzgraf, L. G. *New J. Chem.* **1987**, *11*, 663. (e) Mehrotra, R. C. *J. Non-Cryst. Solids* **1990**, *121*, 1. (f) Bradley, D. C. *Polyhedron* **1994**, *13*, 1111. (g) Chandler, C. D.; Roger, C.; Hampden-Smith, M. J. *Chem. Rev.* **1993**, *93*, 1205. (h) Narula, C. K.; Varshney, A.; Riaz, U. *Chem. Vap. Deposition* **1996**, *2*, 13. (i) Altherr, A.; Wolfgang, H.; Veith, M. *Chem. Vap. Deposition* **1999**, *5*, 87.

of fundamental building blocks, well-defined stoichiometries, and low-temperature (kinetically controlled) routes to metastable structures. In this context, we have been investigating the structure, bonding, and reactivity of tris(*tert*-butoxy)siloxy complexes of the type $L_nE[OSi(O^tBu)_3]_m$ ($n \geq 0$, $m = 1-4$, L_n = amide, alkyl, or alkoxide; E = transition or main-group element).⁵⁻²³ The thermolytic conversions of these well-defined complexes (in the solid state or in nonpolar solvents) occur cleanly and at relatively low temperatures (typically below 200 °C) via the elimination of isobutene and water. We have employed this *thermolytic molecular precursor* method for the low-temperature synthesis of a variety of homogeneous metal–silicon–oxide materials with tailored properties.⁵⁻²³ Other nonhydrolytic routes to mixed-element oxides based on molecular solution chemistry have also been developed. These include the condensation of metal alkoxides with metal acetates²⁴ or metal halides.²⁵

Vanadia–silica materials are important catalytic materials that have been widely studied for the selective oxidation of hydrocarbons, including the conversion of methane to formaldehyde and the oxidative dehydrogenation (ODH) of ethane and propane.²⁶ We have recently examined use of the molecular precursor $OV[OSi(O^tBu)_3]_3$ to prepare homogeneous V/Si/Zr/O materi-

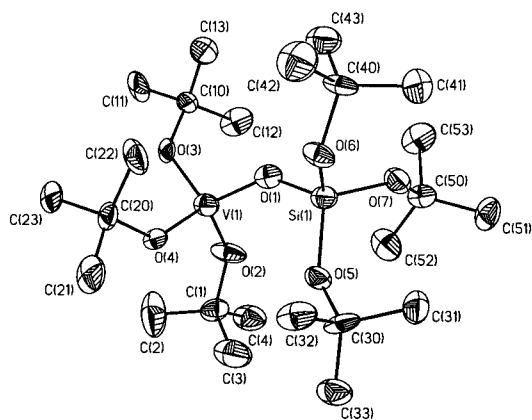


Figure 1. Thermal ellipsoid plot of $(^tBuO)_3VOSi(O^tBu)_3$ (**1**) at the 50% probability level. Hydrogen atoms have been removed for clarity.

als via cothermolyses with a zirconium alkoxide.¹⁴ The materials prepared using this method were shown to be effective catalysts for the ODH of propane to propylene. This vanadium tris(*tert*-butoxy)siloxy complex also proved to be a good molecular model for isolated vanadyl sites on silica.¹⁷

To further probe the use of V/Si/O molecular complexes as precursors to materials and as soluble models, we targeted the synthesis of new heteroelement vanadium alkoxysiloxides based upon the $-OSi(O^tBu)_3$ ligand. We report here the synthesis and characterization of two V(IV) molecular precursors to V/Si/O materials, $(^tBuO)_3VOSi(O^tBu)_3$ (**1**) and $(^tBuO)_2V[OSi(O^tBu)_3]_2$ (**2**).

Results and Discussion

Vanadium (IV) Tris(*tert*-butoxy)siloxy Complexes. The reaction of 1 equiv of $HOSi(O^tBu)_3$ with $V(O^tBu)_4$ in toluene at 80 °C under flowing nitrogen afforded the V(IV) alkoxysiloxy complex $(^tBuO)_3VOSi(O^tBu)_3$ (**1**) (eq 1). The air- and moisture-sensitive blue solid present after removal of the solvent (in vacuo) was dissolved in toluene and crystallized from a mixture of toluene and acetonitrile (3:1) at -30 °C. Analytically pure light blue, platelike crystals were isolated after recrystallization from toluene/acetonitrile (3:1) at -30 °C in moderate yield (45%). The 1H NMR spectrum of **1** contains two broad resonances in a 1:1 ratio at ca. 3.5 and 1.5 ppm, corresponding to the $V(O^tBu)_3$ and $Si(O^tBu)_3$ groups, respectively. For comparison, the 1H NMR (benzene- d_6) spectrum of $V(O^tBu)_4$ exhibits one broad resonance at ca. 3 ppm.

To unequivocally determine the identity of **1**, a single-crystal X-ray structure analysis was performed. The molecular structure of **1** is shown in Figure 1, crystallographic data are given in Table 1, and bond distances and angles are listed in the Supporting Information. The crystals did not diffract well, resulting in a structure with an effective resolution of ca. 1.0 Å. Also, the V–O and Si–O bond distances and the geometry of the V and Si centers are similar enough such that rotation of the molecule by 180° (exchanging V for Si) is possible. The lack of long-range correlation between the interiors of the molecule appears as disorder in the V and Si atom positions. Because of this disorder, the metrical parameters associated with the Si and V atoms are average values and should be treated with caution. A similar

(5) McMullen, A. K.; Tilley, T. D.; Rheingold, A. L.; Geib, S. J. *Inorg. Chem.* **1989**, *28*, 3772.

(6) McMullen, A. K.; Tilley, T. D.; Rheingold, A. L.; Geib, S. J. *Inorg. Chem.* **1990**, *29*, 2228.

(7) Terry, K. W.; Tilley, T. D. *Chem. Mater.* **1991**, *3*, 1001.

(8) Terry, K. W.; Gantzel, P. K.; Tilley, T. D. *Chem. Mater.* **1992**, *4*, 1290.

(9) Terry, K. W.; Gantzel, P. K.; Tilley, T. D. *Inorg. Chem.* **1993**, *32*, 5402.

(10) Terry, K. W.; Lugmair, C. G.; Gantzel, P. K.; Tilley, T. D. *Chem. Mater.* **1996**, *8*, 274.

(11) Su, K.; Tilley, T. D.; Sailor, M. J. *J. Am. Chem. Soc.* **1996**, *118*, 3459.

(12) Su, K.; Tilley, T. D. *Chem. Mater.* **1997**, *9*, 588.

(13) Terry, K. W.; Lugmair, C. G.; Tilley, T. D. *J. Am. Chem. Soc.* **1997**, *119*, 9745.

(14) Rulkens, R.; Tilley, T. D. *J. Am. Chem. Soc.* **1998**, *120*, 9959.

(15) Lugmair, C. G.; Tilley, T. D. *Inorg. Chem.* **1998**, *37*, 764.

(16) Terry, K. W.; Su, K.; Tilley, T. D.; Rheingold, A. L. *Polyhedron* **1998**, *17*, 891.

(17) Rulkens, R. R.; Male, J. L.; Terry, K. W.; Olthoff, B.; Khodakov, A.; Bell, A. T.; Iglesia, E.; Tilley, T. D. *Chem. Mater.* **1999**, *11*, 2966.

(18) Coles, M. P.; Lugmair, C. G.; Terry, K. W.; Tilley, T. D. *Chem. Mater.* **2000**, *12*, 122.

(19) Male, J. L.; Niessen, H. G.; Bell, A. T.; Tilley, T. D. *J. Catal.* **2000**, *194*, 431.

(20) Kriesel, J. W.; Tilley, T. D. *J. Mater. Chem.* **2001**, *11*, 1081.

(21) Furdala, K. L.; Tilley, T. D. *Chem. Mater.* **2001**, *13*, 1817.

(22) Furdala, K. L.; Tilley, T. D. *J. Am. Chem. Soc.* **2001**, *123*, 10133.

(23) Lugmair, C. G.; Furdala, K. L.; Tilley, T. D. *Chem. Mater.*, ASAP on web.

(24) Jansen, M.; Guenther, E. *Chem. Mater.* **1995**, *7*, 2110.

(25) Vioux, A. *Chem. Mater.* **1997**, *9*, 2292.

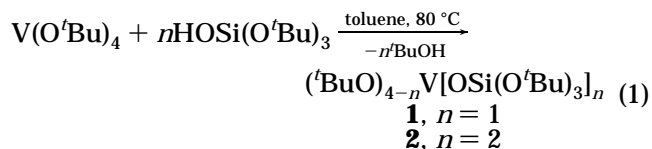
(26) (a) Liu, H.-F.; Liu, R.-S.; Liew, K. Y.; Johnson, R. E.; Lunsford, J. H. *J. Am. Chem. Soc.* **1984**, *106*, 4117. (b) Lische, G.; Hanke, W.; Jerschekewitz, H. G.; Ohlmann, J. *J. Catal.* **1985**, *91*, 54. (c) Zhen, K. J.; Mark, C. H.; Lewis, K. B.; Somorjai, G. A. *J. Catal.* **1985**, *94*, 501. (d) Jonson, B.; Rebenstrof, B.; Larsson, R.; Andersson, S. L. *J. Chem. Soc., Faraday Trans.* **1988**, *84*, 1897. (e) Spencer, N. D.; Pereira, C. J. *J. Catal.* **1989**, *116*, 399. (f) Mamedov, E. A.; Corberán, C. *Appl. Catal. A* **1995**, *127*, 1. (g) Iruata, S.; Cornaglia, L. M.; Miro, E. E.; Lombardo, E. A. *J. Catal.* **1995**, *156*, 167. (h) Albonetti, S.; Cavani, F.; Trifirò, F. *Catal. Rev.-Sci. Eng.* **1996**, *38*, 413. (i) Centi, G.; Trifirò, F. *Appl. Catal. A* **1996**, *143*, 3. (j) Parmaliana, A.; Sokolovskii, V.; Arena, F.; Frusteri, F.; Miceli, D. *Catal. Lett.* **1996**, *40*, 105. (k) Puglisi, M.; Arena, F.; Frusteri, F.; Sokolovskii, V.; Parmaliana, A. *Catal. Lett.* **1996**, *41*, 41. (l) Sun, Q.; Jehng, J. M.; Hu, H. H.; Herman, R. G.; Wachs, I. E.; Klier, K. *J. Catal.* **1997**, *165*, 91. (m) Banares, M.; Gao, X.; Fierro, J. L. G.; Wachs, I. E. *Stud. Surf. Sci. Catal.* **1997**, *110*, 295. (n) Martra, G.; Arena, F.; Coluccia, S.; Frusteri, F.; Parmaliana, A. *Catal. Today* **2000**, *63*, 197.

Table 1. Crystallographic Data for Complexes 1 and 2

	(^t BuO) ₃ VOSi(O ^t Bu) ₃ (1)	(^t BuO) ₂ V[OSi(O ^t Bu) ₃] ₂ (2)
formula	C ₂₄ H ₅₄ O ₇ SiV	C ₃₂ H ₇₂ O ₁₀ Si ₂ V
cryst size (mm)	0.22 × 0.12 × 0.03	0.23 × 0.16 × 0.07
morphology	plate	needle
cryst syst.	monoclinic	monoclinic
space group	<i>P</i> 2 ₁ / <i>n</i> (#14)	<i>P</i> 2 ₁ / <i>n</i> (#14)
<i>Z</i>	4	4
cell constants		
<i>a</i> (Å)	9.669(3)	9.616(2)
<i>b</i> (Å)	16.446(6)	16.597(3)
<i>c</i> (Å)	20.417(7)	27.803(6)
β (deg)	94.94(6)	96.78(3)
<i>V</i> (Å ³)	3234(2)	4406(2)
<i>D</i> _{calc} (g cm ⁻³)	1.096	1.091
<i>F</i> ₀₀₀	1164	1580
μ (Mo Kα) (cm ⁻¹)	3.8	3.2
radiation	Mo Kα (0.70169 Å)	Mo Kα (0.70169 Å)
2θ max (deg)	41.1	46.8
scan type	ω (0.3° per frame)	ω (0.3° per frame)
temp (°C)	-142	-112
exposure time	30 s per frame	30 s per frame
measured refs.	10445	19380
unique refs.	3468	7355
<i>R</i> _{obs} , <i>R</i> _{all}	0.060, 0.187	0.047, 0.122
<i>wR</i> _{2obs}	0.102, 0.132	0.096, 0.108
<i>wR</i> _{2all}		
GOF _{obs} , GOF _{all}	1.104, 0.823	1.058, 0.780

disorder was observed in the analogous Cr(IV) complex (^tBuO)₃CrOSi(O^tBu)₃.²¹

The reaction of 2 equiv of HOSi(O^tBu)₃ with V(O^tBu)₄ in toluene at 80 °C under flowing nitrogen afforded (O^tBu)₂V[OSi(O^tBu)₃]₂ (**2**) (eq 1). The bright blue air- and moisture-sensitive compound was purified by crystallization from a mixture of toluene and acetonitrile (3:1) at -30 °C (61% yield). The ¹H NMR spectrum of **2** contains two broad resonances in a 1:3 ratio at ca. 4.5 and 1.5 ppm, corresponding to the V(O^tBu) and OSi(O^tBu)₃ groups, respectively.



The identity of **2** was confirmed by a single-crystal X-ray crystallographic study. The molecular structure of **2** is shown in Figure 2, crystallographic data are given in Table 1, and bond distances and angles are listed in the Supporting Information. The V–O(Si) distances of 1.779(2) and 1.781(2) Å are slightly longer than the V–O(C) distances (1.757(2) and 1.758(2) Å). For comparison, the gas-phase electron diffraction structure of V(O^tBu)₄ revealed an average V–O bond distance of 1.779(6) Å.²⁷ The V–O(Si) distances in OV[OSi(O^tBu)₃]₃,¹⁷ as estimated by comparison of the Raman stretching frequencies with a series of reference compounds,²⁸ and by an EXAFS study¹⁷ were 1.82 and 1.77 Å, respectively. The V–O(Si) distances in OV[OSiPh₃]₃

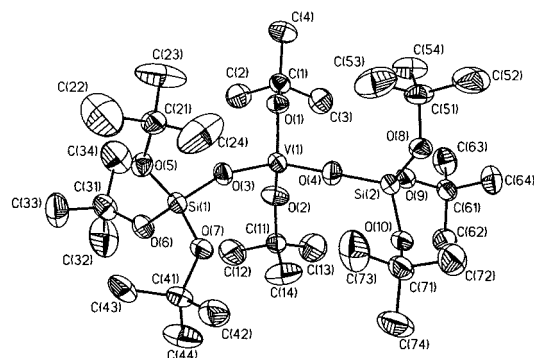


Figure 2. Thermal ellipsoid plot of (^tBuO)₂V[OSi(O^tBu)₃]₂ (**2**) at the 50% probability level. Hydrogen atoms have been removed for clarity.

were found to be 1.742(2) Å by X-ray crystallography.²⁹ In general, comparable metrical parameters in **1** and **2** appear to be similar.

The IR spectra of **1** and **2** are nearly identical to those of their isostructural Cr(IV) analogues,²¹ with peaks at ca. 1065 cm⁻¹ assigned to Si–O–C vibrations, and vibrations at ca. 920 and 910 cm⁻¹ derived from the V–O–Si linkages.^{17,30} The vibrations at ca. 940, 790, and 610 cm⁻¹ in **1** and **2** are likely associated with the VO^tBu groups.³¹ Room-temperature electron paramagnetic resonance (EPR) spectra of complexes **1** and **2** (as solutions in *n*-octane) revealed eight lines, indicative of ⁵¹V hyperfine splitting (spin = 7/2). The isotropic *g* values of 1.974(3) for **1** (*A* = 70(1) G) and 1.973(4) for **2** (*A* = 72(3) G) are consistent with the presence of 1 unpaired electron and are similar to values reported for other V(IV) distorted tetrahedral complexes.^{32,33}

Solid-State Thermolyses of 1 and 2. The solid-state thermolytic conversions of **1** and **2** to ceramic materials were examined under inert (N₂) conditions. The thermogravimetric analysis (TGA) traces for **1** and **2** under an atmosphere of N₂ are shown in Figure 3. The onset of decomposition occurred at ca. 100 °C for both **1** and **2** and was followed by a precipitous mass loss in each case. The ceramic yield for the decomposition of **1** was 27.8%, which is intermediate between the values expected for VO₂·SiO₂ (26.8%) and VO_{2.5}·SiO₂ (28.3%). The ceramic yield for the decomposition of **2** (25.9%) was somewhat lower than the calculated values for VO₂·2SiO₂ (28.1%) and VO_{2.5}·2SiO₂ (29.2%).

No endothermic transition (e.g., for melting) was observed prior to the endotherm for decomposition of **1** (by differential scanning calorimetry, DSC). The DSC analysis for complex **2** revealed a small endothermic

(28) Hardcastle, F. D.; Wachs, I. E. *J. Phys. Chem.* **1991**, *95*, 5031.

(29) Feher, F. J.; Walzer, J. F.; *Inorg. Chem.* **1991**, *30*, 1689.

(30) (a) Rice, G. L.; Scott, S. L. *Langmuir* **1997**, *13*, 1545. (b) Rice, G. L.; Scott, S. L. *J. Mol. Catal. A: Chem.* **1997**, *125*, 73.

(31) IR data for V(O^tBu)₄: 2973 vs, 2928 m, 2901 w, 2871 w, 1470 w, 1457 w, 1385 m, 1362 s, 1233 m, 1172 s, 1027 w sh, 939 vs, 909 w sh, 787 s, 614 s, 476 w.

(32) (a) Bradley, D. C.; Moss, R. H.; Sales, K. D. *Chem. Commun.* **1969**, 1255. (b) Bradley, D. C.; Rendall, I. F.; Sales, K. D. *J. Chem. Soc. Dalton* **1973**, 2228. (c) Alyea, E. C.; Bradley, D. C. *J. Chem. Soc. (A)* **1969**, 2330. (d) Razuvaev, G. A.; Latyaeva, V. N.; Drobotenko, V. V.; Linyova, A. N.; Vishinskaya, L. I.; Cherkasov, V. K. *J. Organomet. Chem.* **1977**, *131*, 43. (e) Heinrich, D. D.; Folting, K.; Huffman, J. C.; Reynolds, J. G.; Christou, G. *Inorg. Chem.* **1991**, *30*, 300.

(33) For further comparison, the EPR spectrum of V(O^tBu)₄ at room temperature in *n*-octane was measured, *g* = 1.975(3) and *A* = 69(2) G, consistent with the literature values: Kokoszka, G. F.; Allen, H. C., Jr.; Gordon, G. *Inorg. Chem.* **1966**, *5*, 91.

(27) Haaland, A.; Rypdal, K.; Volden, H. V.; Andersen, R. A. *J. Chem. Soc., Dalton Trans.* **1992**, 891.

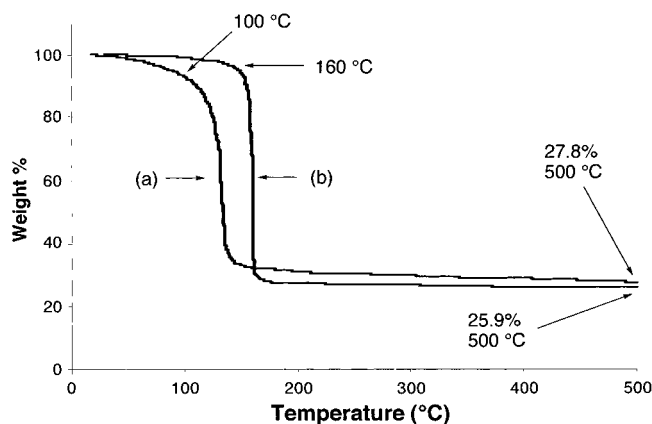


Figure 3. TGA traces in N_2 with a heating rate of $10\text{ }^\circ\text{C min}^{-1}$ for (a) **1** and (b) **2**.

Table 2. Hydrolyses of 1 and 2^a

product	1 obsvd (theor)	2 obsvd (theor)
$t\text{-BuOH}$	3.3 (3)	1.8 (2)
$\text{HOSi}(\text{O}^i\text{Bu})_3$	1.3 (1)	2.1 (2)

^a Equiv based upon **1** and **2**. The error is estimated to be $\pm 10\%$.

Table 3. Solution Thermolyses of 1 and 2 after 1 h^a

product	1 obsvd (theor)	2 obsvd (theor)
CH_2CMe_2	4.4 (6)	6.1 (8)
$t\text{-BuOH}$	trace (0)	0.2 (0)
$\text{HOSi}(\text{O}^i\text{Bu})_3$	0.3 (0)	0.5 (0)

^a Equiv based upon **1** and **2**. The error is estimated to be $\pm 10\%$.

transition at ca. $60\text{ }^\circ\text{C}$, well before that observed for the thermal decomposition. This endotherm corresponds closely to the melting point of $\text{HOSi}(\text{O}^i\text{Bu})_3$ ($65\text{ }^\circ\text{C}$). It is evident that the brief exposure to air during sample transfer to the instrument leads to the formation of small amounts of $\text{HOSi}(\text{O}^i\text{Bu})_3$ (via hydrolysis), which melts and boils away on heating, thus leading to the slightly low ceramic yield for **2**. A traditional melting point determination (sealed capillary tube under N_2) revealed no melting behavior for **2** prior to decomposition.

Hydrolyses of 1 and 2. Samples of **1** or **2** in the presence of a measured amount of ferrocene as a standard were dissolved in benzene- d_6 and hydrolyzed by the addition of $5\text{ }\mu\text{L}$ of H_2O via a syringe. The hydrolysis products were identified (by ^1H NMR spectroscopy) as *tert*-butyl alcohol and tris(*tert*-butoxy)silanol (Table 2). The relative amounts of each product are in good agreement with the predicted values. These results clearly suggest that a sol-gel route to a V/Si/O material using either **1** or **2** would lead to cleavage of the V–O–Si linkage early in the gelation process.

^1H NMR Studies of the Thermal Decompositions of 1 and 2. To investigate the chemical transformation associated with the conversions of **1** and **2** to V/Si/O materials, the soluble products from their thermal decompositions in benzene- d_6 were quantified by room temperature ^1H NMR spectroscopy after a short period of heating (1 h). Integration against a ferrocene standard revealed that the major product in both cases was isobutene, and small amounts of *tert*-butyl alcohol and tris(*tert*-butoxy)silanol were also observed (Table 3). Two overlapping resonances (at 0.86 and 0.84 ppm) observed in the ^1H NMR spectra after completion of the ther-

molyses of **1** and **2** correspond to very small amounts of products that could not be identified (by NMR spectroscopy or GC-MS analysis).

The observation of only trace amounts of water as a product in the thermolyses (by ^1H NMR spectroscopy) is attributed to the formation of an oxide material that acts as a desiccant to remove the H_2O from solution. It is also assumed that some of the H_2O is responsible for formation of the small amounts of $\text{HOSi}(\text{O}^i\text{Bu})_3$ and $t\text{-BuOH}$ that are observed. Prolonged thermolyses (12 h) led to decomposition of the remaining $\text{HOSi}(\text{O}^i\text{Bu})_3$, via the elimination of CH_2CMe_2 and $t\text{-BuOH}$. The detection of slightly less than stoichiometric amounts of $t\text{-Bu}$ groups can be attributed to the presence of isobutene in the gas phase and to formation of the unidentified species (vide supra).

Syntheses of V/Si/O Materials from 1 and 2. The ease of preparation of **1** and **2** and their low thermolysis temperatures suggested that these complexes should be well-suited for the large-scale syntheses of V/Si/O materials via thermolytic molecular precursor routes. To that end, solid-state thermolyses of **1** and **2** were performed by heating evacuated thick-walled Pyrex pyrolysis tubes containing the precursor in a preheated oven at $180\text{ }^\circ\text{C}$ for 18 h. The as-synthesized materials from the solid-phase thermolyses of both **1** (**VOSi1_{ss}**) and **2** (**VOSi2_{ss}**) were dark brown in color.

The high solubility of **1** and **2** in organic solvents allowed us to use these molecular precursors to synthesize V/Si/O xerogels from solution-phase thermolyses. The thermal decomposition of *n*-octane solutions of **1** (0.1 M) at $180\text{ }^\circ\text{C}$ over 24 h led to the formation of dark brown gels that, upon air-drying, afforded the xerogel **VOSi1_{xg}**. Similar treatments of *n*-octane solutions of **2** (0.1 M) produced the light brown xerogel **VOSi2_{xg}**. Elemental analyses of **VOSi1_{xg}** and **VOSi2_{xg}** revealed that the V/Si ratios were 1:0.9 and 1:2.3, respectively, indicating approximate retention of the stoichiometry of the precursors. All of the materials obtained from **1** and **2** were ground to fine powders and calcined in O_2 (100 mL min^{-1}) at various temperatures. For comparison, the xerogel obtained from a solution thermolysis of $\text{OV}[\text{OSi}(\text{O}^i\text{Bu})_3]_3$ (**VOSi3_{xg}**) was examined similarly.

The crystallization behaviors of **VOSi1_{ss}**, **VOSi2_{ss}**, **VOSi1_{xg}**, **VOSi2_{xg}**, and the xerogel derived from $\text{OV}[\text{OSi}(\text{O}^i\text{Bu})_3]_3$ (**VOSi3_{xg}**) were monitored by powder X-ray diffraction (PXRD) analysis after calcination in O_2 at $100\text{ }^\circ\text{C}$ intervals (Table 4). Interesting differences were observed in the temperatures at which the crystallization of V_2O_5 was first observed and in the estimated size of the V_2O_5 crystallites (using the Scherrer method³⁴). For the materials derived from the solid-state thermolyses of **1** and **2** (**VOSi1_{ss}** and **VOSi2_{ss}**), crystalline V_2O_5 was first observed after calcination at $400\text{ }^\circ\text{C}$, as evidenced by the appearance of reflections attributed to V_2O_5 . The peaks were significantly more intense and narrower after calcination at $500\text{ }^\circ\text{C}$, indicating the presence of increased amounts of larger V_2O_5 crystallites. The xerogels derived from **1** and **2** (**VOSi1_{xg}** and **VOSi2_{xg}**) exhibited PXRD patterns (Figure 4) that are similar to those of the materials derived from the solid-state thermolyses in that they appeared

Table 4. Summary of the PXRD Data for the V/Si/O Materials

sample ^a	V ₂ O ₅ crystallite diameter (nm) ^b	relative V ₂ O ₅ content ^c	sample color
VOSi1_{xg}			
200 °C	amorphous	amorphous	brown
300 °C	amorphous	amorphous	yellow
400 °C	17	1.0	yellow
500 °C	19	1.0	orange
VOSi2_{xg}			
200 °C	amorphous	amorphous	yellow/brown
300 °C	amorphous	amorphous	yellow
400 °C	34	0.49	yellow
500 °C	44	0.48	orange
VOSi3_{xg}			
200 °C	amorphous	amorphous	green/yellow
300 °C	46	N/A	yellow
400 °C	60	0.76	yellow
500 °C	73	0.38	yellow
VOSi1_{ss}			
200 °C	amorphous	amorphous	yellow/brown
300 °C	amorphous	amorphous	yellow/brown
400 °C	24	0.47	yellow
500 °C	32	0.53	orange
VOSi2_{ss}			
200 °C	amorphous	amorphous	brown
300 °C	amorphous	amorphous	yellow/brown
400 °C	49	0.60	orange
500 °C	51	0.46	orange

^a The temperature is that of the calcination temperature (O₂, 2 h) of the indicated material. ^b Average values (Scherrer method) after correcting for instrument broadening and rounded to the nearest nm. ^c Amount of V₂O₅ relative to that in **VOSi1_{xg}** using the area under the PXRD peak at 2θ = 26°.

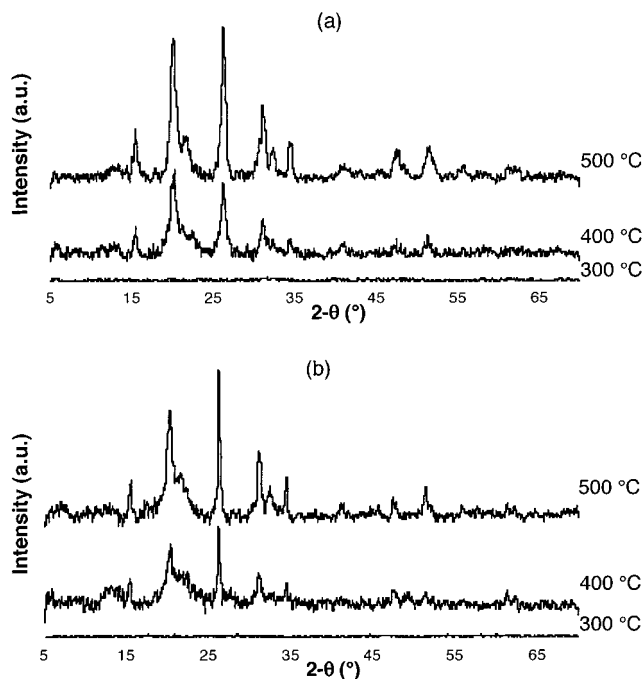


Figure 4. Room-temperature PXRD diffractograms of the xerogels derived from solution thermolyses of **1** and **2** (**VOSi1_{xg}** and **VOSi2_{xg}**, respectively) after calcination under a flow of O₂ (100 cm³ min⁻¹) at 100 °C intervals. (a) **VOSi1_{xg}**. (b) **VOSi2_{xg}**.

amorphous after calcination at 300 °C, with nanocrystalline V₂O₅ being present only after treatment at 400 °C. In contrast, the xerogel derived from OV[OSi(O^t-Bu)₃]₃ (**VOSi3_{xg}**) exhibited strong reflections for V₂O₅ in the PXRD pattern after calcination at 300 °C (Figure 5). The crystallite sizes were much larger for this sample

than for the others. The xerogel **VOSi1_{xg}** contains the smallest nanocrystals of V₂O₅ and **VOSi3_{xg}** clearly contains the largest domains of nanocrystalline V₂O₅ after calcination at both 400 and 500 °C. This trend is opposite to what might be expected based solely upon the vanadium contents of the molecular precursors. In fact, calcination at a higher temperature (500 °C) shows that **VOSi1_{xg}** produces the largest quantity of V₂O₅ (in the form of smaller crystallites) while **VOSi3_{xg}** contains the least amount of V₂O₅ (qualitatively, based upon the area under the PXRD peaks).

It is known that the formation of V₂O₅ domains in V/Si/O materials is facilitated under aqueous conditions^{26f,35} and that hydrated vanadium oxide species are efficiently converted to V₂O₅ in the presence of SiO₂.^{35a,36} However, four-coordinate vanadium species within ordered silica materials are not as readily converted to V₂O₅.³⁷ Stiegman et al. have recently shown that the homogeneity of sol-gel-derived vanadia-silica xerogels is highly dependent upon the specific gelation conditions.³⁸ For example, the amount of water present during sol-gel preparations of vanadia-silica xerogels dramatically alters the homogeneity of the final material, with lower water content giving rise to more homogeneous xerogels.^{38a} Further, reduction of the vanadium species (from V(V) to V(IV)) during the gelation was shown to increase the amount of vanadium that could be homogeneously incorporated into the final material.^{38b}

The later formation of V₂O₅ for the xerogels derived from the V(IV) precursors **1** and **2** (which produce more water than OV[OSi(O^t-Bu)₃]₃ upon thermolysis) illustrates the large effect that the nature of the precursor can have on the properties of materials derived therefrom. Previously, the cleavage of V-O-Si linkages via hydrolysis (from H₂O evolved during thermolysis) was invoked to explain the formation of V₂O₅ after calcination of **VOSi3_{xg}** at low temperatures.¹⁷ The results presented here therefore suggest that the oxidation state of vanadium may be a more important factor than water content in determining the crystallization behavior of the V/Si/O system. Larger crystallites of V₂O₅ also seem to result from higher silicon content in the precursor complex.

Interestingly, the materials derived from the solid-state thermolyses of **1** and **2** (**VOSi1_{ss}** and **VOSi2_{ss}**) contain slightly larger V₂O₅ crystallites than their xerogel counterparts. The relative amount of V₂O₅ present in **VOSi1_{ss}** is approximately half that of **VOSi1_{xg}**, whereas **VOSi2_{ss}** contains a similar amount of crystalline V₂O₅ relative to **VOSi2_{xg}** (Table 4). This

(35) (a) van der Voort, P.; White, M. G.; Mitchell, M. B.; Verberckmoes, A. A.; Vansant, E. F. *Spectrochim. Acta A* **1997**, *53*, 2181. (b) Inumaru, K.; Misono, M.; Okuhara, T. *Appl. Catal. A* **1997**, *149*, 133. (c) Dutoit, D. C. M.; Schneider, M.; Baiker, A. *Chem. Mater.* **1996**, *8*, 734.

(36) (a) Went, G. T.; Oyama, S. T.; Bell, A. T. *J. Phys. Chem.* **1990**, *94*, 4240. (b) Dutoit, D. C. M.; Schneider, M.; Fabrizioli, P.; Baiker, A. *J. Mater. Chem.* **1997**, *7*, 271. (c) Jheng, J.-M.; Deo, G.; Weckhuysen, B. M.; Wachs, I. E. *J. Mol. Catal. A* **1996**, *110*, 41. (d) Morey, M.; Davidson, A.; Eckert, H.; Stucky, G. *Chem. Mater.* **1996**, *8*, 486.

(37) (a) Kornatowski, J.; Wichterlová, B.; Jirkovsky, J.; Löffler, E.; Pilz, W. *J. Chem. Soc., Faraday Trans.* **1996**, *92*, 1067. (b) Zhang, S. G.; Higashimoto, S.; Yamashita, H.; Anpo, M. *J. Phys. Chem. B* **1998**, *102*, 5590.

(38) (a) Curran, M. D.; Pooré, D. D.; Stiegman, A. E. *Chem. Mater.* **1998**, *10*, 3156. (b) Curran, M. D.; Gedris, T. E.; Stiegman, A. E. *Chem. Mater.* **1999**, *11*, 1120. (c) Curran, M. D.; Stiegman, A. E. *J. Phys. Chem. B* **2000**, *104*, 8338.

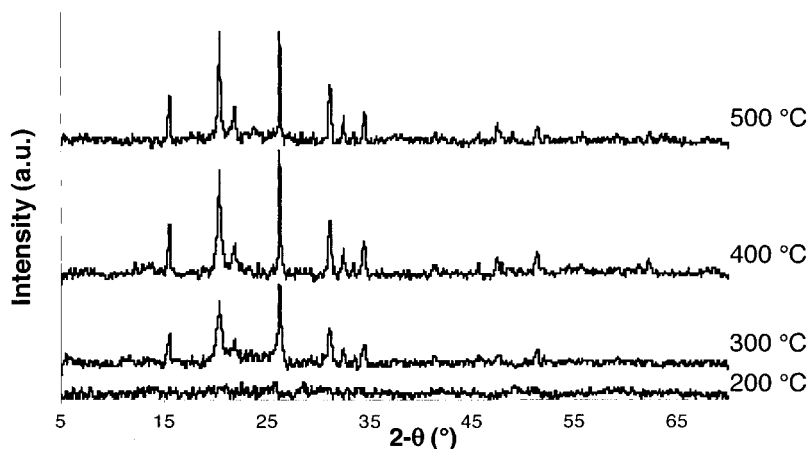


Figure 5. Room-temperature PXRD diffractograms of the xerogel derived from the solution thermolysis of $\text{OV}[\text{OSi}(\text{O}'\text{Bu})_3]_3$ after calcination under a flow of O_2 ($100 \text{ cm}^3 \text{ min}^{-1}$) at 100°C intervals.

implies that initially formed VOSi1_{ss} may be more homogeneous than as-synthesized VOSi1_{yg} and that VOSi2_{ss} and VOSi2_{yg} have similar initial degrees of homogeneity. Note that the solid-phase thermolysis of the Cr analogue of **1** also yielded a material that appeared to be more homogeneous than the xerogel derived from its solution-phase thermolysis.²¹

Thermogravimetric analyses of VOSi1_{yg} , VOSi2_{yg} , and VOSi3_{yg} (after an initial pretreatment at 200°C) in O_2 with a heating rate of $10^\circ\text{C min}^{-1}$ revealed mass losses of 9.9, 9.9, and 7.3%, respectively. These mass losses presumably result from removal of adsorbed H_2O and residual organic species and occur in two stages with ca. 50% of the total loss occurring between room temperature and 300°C . These events probably correspond to physisorbed and chemisorbed H_2O , respectively, with residual organic species being lost throughout the heating process.

Differential scanning calorimetric (DSC) analyses of these xerogels provided further insight into the changes that occur upon calcination. Each material exhibited an exothermic transition that initiated below 300°C and is associated with the crystallization of V_2O_5 .¹⁷ The onsets of the exothermic transitions were at 290°C (VOSi1_{yg}), 260°C (VOSi2_{yg}), and 225°C (VOSi3_{yg}). The energy associated with this transition was largest for VOSi3_{yg} (390 J g^{-1}) and smallest for VOSi2_{yg} (100 J g^{-1}). The exothermic transition associated with VOSi1_{yg} was 225 J g^{-1} . The lower onset temperature for the exothermic transition in VOSi3_{yg} follows what would be expected based upon the PXRD data. Despite the lack of V_2O_5 detection in VOSi1_{yg} and VOSi2_{yg} after calcination at 300°C (by PXRD), the DSC exotherm suggests a significant reorganization prior to this temperature, possibly due to the formation of small V_2O_5 domains. Although no such domains were observed by Raman spectroscopy, these experiments may have been complicated by fluorescence due to the high vanadium content of the materials.^{21,39} No further exothermic events were observed for any of the samples (by DSC), which is an indication that the further growth of V_2O_5 crystallites is gradual after the initial nucleation. An endothermic transition associated with the melting of V_2O_5 (ca. 655°C) was observed for all of the xerogels:

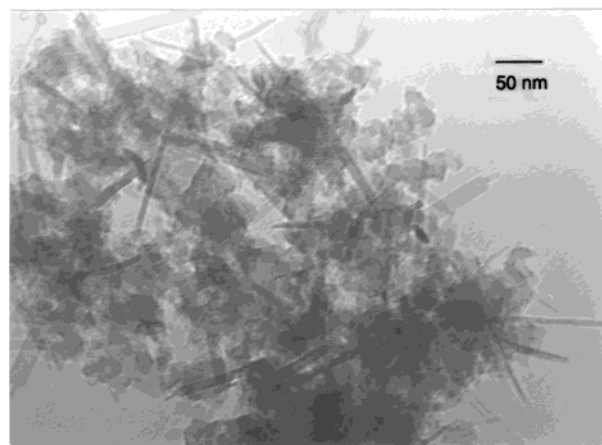


Figure 6. TEM image of VOSi1_{yg} after calcination in O_2 ($100 \text{ cm}^3 \text{ min}^{-1}$) at 500°C .

VOSi1_{yg} (39 J g^{-1}), VOSi2_{yg} (33 J g^{-1}), VOSi3_{yg} (25 J g^{-1}). The trend of increasing heat flow (for the melting of V_2O_5) with increasing vanadium content in the precursor is consistent with the relative amounts of V_2O_5 determined by PXRD.

Transmission electron microscopy (TEM) was used to further characterize the materials obtained from **1** and **2**. For comparison, TEM images of VOSi3_{yg} were also obtained. The micrographs of VOSi1_{yg} , after calcination at 500°C (Figure 6), revealed the presence of a large number of V_2O_5 crystallites growing from an amorphous matrix. The crystallites were elongated along one direction to give them a rod- or needlelike appearance. The nanocrystals that could be discerned from the matrix appeared to be quite uniform in size. Measuring the size of the crystallites in several different areas throughout the sample determined that the average dimensions for these crystallites were ca. $10 \times 90 \text{ nm}$ (rounded to the nearest 5 nm to reflect the error in measurement). The TEM images of VOSi2_{yg} , after calcination at 500°C (Figure 7), revealed fewer crystallites and average dimensions of $20 \times 95 \text{ nm}$. In agreement with the trend observed in the PXRD studies, the TEM images of VOSi3_{yg} , after calcination at 500°C (Figure 8), revealed few crystallites; however, these were well-formed, had similar sizes, and were rather large (average dimensions of $50 \times 80 \text{ nm}$).

(39) Weckhuysen, B. M.; Wachs, I. E. *J. Phys. Chem.* **1996**, *100*, 14437.

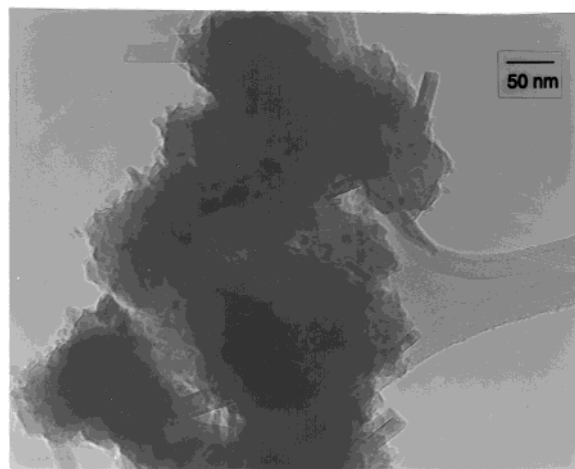


Figure 7. TEM image of **VOSi2_{xg}** after calcination in O₂ (100 cm³ min⁻¹) at 500 °C.

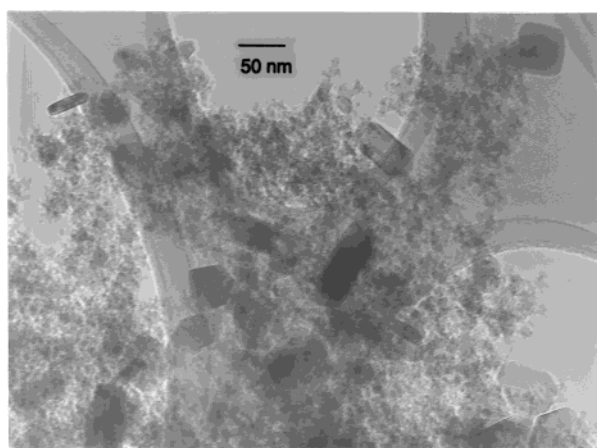


Figure 8. TEM image of **VOSi3_{xg}** after calcination in O₂ (100 cm³ min⁻¹) at 500 °C.

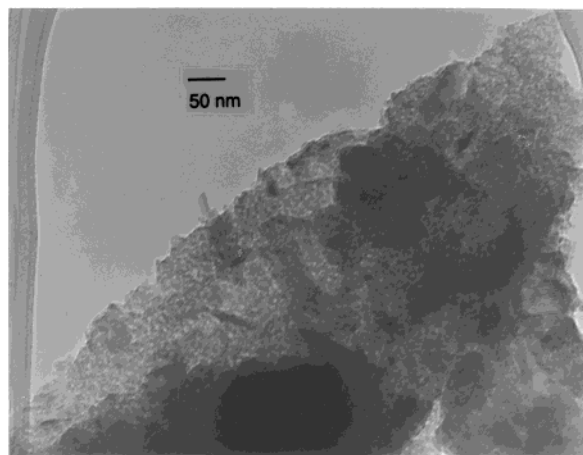


Figure 9. TEM image of **VOSi2_{ss}** after calcination in O₂ (100 cm³ min⁻¹) at 500 °C.

The TEM micrographs of the solid-state-derived materials, **VOSi1_{ss}** and **VOSi2_{ss}**, were markedly different from those of the xerogels and appear to reveal large amorphous particles with V₂O₅ crystallites (vide infra) encased within. The TEM images for both of these materials were quite similar, and Figure 9 presents a representative image for **VOSi2_{ss}**. Although the PXRD patterns for **VOSi1_{ss}** and **VOSi2_{ss}** reveal only the presence of crystalline V₂O₅, the lack of a significant

Table 5. N₂ Porosimetry Data for the Materials Derived from **1** and **2**

sample ^a	BET surface area (m ² g ⁻¹) ^b	total pore volume (cm ³ g ⁻¹) ^c	average pore radius (Å) ^d
VOSi1_{xg}			
300 °C	40	0.06	30
400 °C	10	0.04	80
500 °C	5	0.04	115
VOSi2_{xg}			
300 °C	70	0.27	75
400 °C	60	0.23	75
500 °C	55	0.23	80
VOSi1_{ss}			
300 °C	30	0.06	40
400 °C	10	0.05	95
500 °C	5	0.04	110
VOSi2_{ss}			
300 °C	170	0.20	25
400 °C	100	0.15	30
500 °C	65	0.15	45

^a The temperature is that of the calcination temperature (O₂, 2 h) of the indicated material. ^b Rounded to the nearest 5 m² g⁻¹ to reflect the approximate error in measurement. ^c Rounded to the nearest 0.01 cm³ g⁻¹ to reflect the error in measurement. ^d Calculated using the 2PV/area method and rounded to the nearest 5 Å.

number of visible V₂O₅ crystallites implies that the vanadium species are contained within the matrix and may be evenly dispersed.

The surface areas and porosities of the materials derived from **1** and **2** were investigated by N₂ porosimetry (Table 5). Surface area measurements were obtained by means of the Brunauer–Emmet–Teller (BET) method⁴⁰ and pore size distributions were analyzed by the Barrett–Joyner–Halenda (BJH) method.⁴¹ The N₂ adsorption–desorption isotherms for the xerogel and solid-state-derived materials from **1** (**VOSi1_{xg}** and **VOSi1_{ss}**) and the xerogel from **2** (**VOSi2_{xg}**) resembled those of type II, indicating that much of the pore volume arises from macroporosity.⁴² The N₂ adsorption–desorption isotherm for **VOSi2_{xg}** is given in Figure 10a. In contrast, the N₂ adsorption–desorption isotherm for the material derived from the solid-state thermolysis of **2** (**VOSi2_{ss}**) appeared to be closer to that of type 1 with type H4 hysteresis (Figure 10b), indicating the presence of narrow slitlike micropores.⁴² The BET surface areas of **VOSi1_{xg}** and **VOSi1_{ss}** were quite low after calcination, even at low temperatures (Table 5). The BET surface areas of **VOSi2_{xg}** and **VOSi2_{ss}** were greater than their **VOSi1** counterparts, with **VOSi2_{ss}** exhibiting a much higher surface area. With the exception of **VOSi2_{ss}**, the surface areas of the materials derived from **1** and **2** are uncharacteristically low for materials generated via thermolytic molecular precursor routes. For comparison, the materials generated from the Cr analogue of **1** (both solid and solution-phase thermolyses) had surface areas that were much higher (ca. 300 m² g⁻¹)²¹ and xerogels generated from the solution thermolysis of Zr[OSi(OⁱBu)₃]₄ possess surface areas of ca. 700 m² g⁻¹.¹³ We attribute the relatively low surface areas observed for the V/Si/O materials derived from **1**

(40) Brunauer, S.; Emmett, P. H.; Teller, E. *J. Am. Chem. Soc.* **1938**, *60*, 309.

(41) Barrett, E. P.; Joyner, L. G.; Halenda, P. P. *J. Am. Chem. Soc.* **1951**, *73*, 373.

(42) Sing, K. S. W.; Everett, D. H.; Haul, R. A.; Moscou, L.; Pierotti, R. A.; Rouquerol, J.; Siemieniowska, T. *Pure Appl. Chem.* **1985**, *57*, 603.

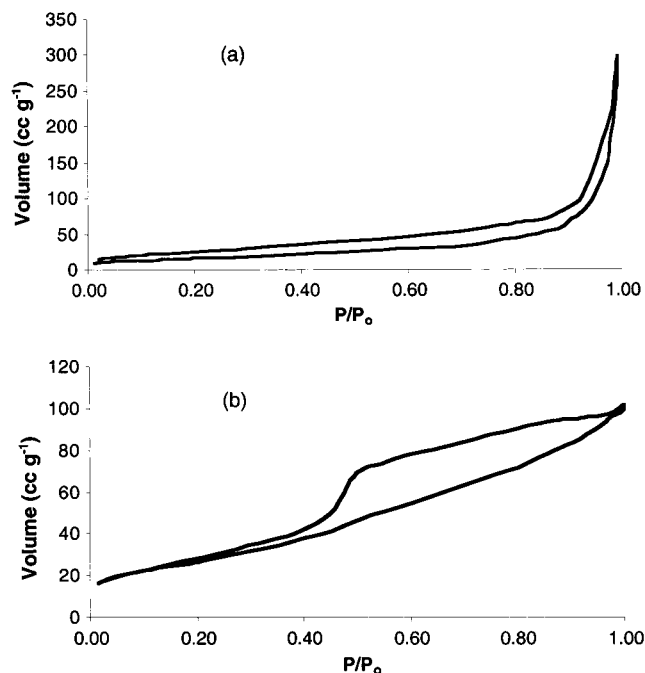


Figure 10. Nitrogen adsorption-desorption isotherms after calcination at 300 °C in O₂ for (a) **VOSi2_{xg}** and (b) **VOSi2_{ss}**.

and **2** to both the low silicon content and the observed crystallization of V₂O₅. Although **VOSi3_{xg}** undergoes phase separation much earlier than the materials derived from **1** and **2**, the high silicon content appears to result in a greater surface area, even after calcination at 500 °C (ca. 300 m² g⁻¹).¹⁷

Conclusions

Two new single-source molecular precursors for V/Si/O materials, (tBuO)₃VOSi(O^tBu)₃ (**1**) and (tBuO)₂V[OSi(O^tBu)₃]₂ (**2**), were synthesized and structurally characterized. These complexes are soluble molecular models for vanadium(IV) centers dispersed within a silica matrix, given the presence of V–O–Si linkages and the oxygen environments of the vanadium and silicon centers. These molecular precursors were used to generate materials of the approximate formulas VO_{2.5}SiO₂ and VO_{2.5}·2SiO₂ via two thermolytic routes (solid-state and solution thermolyses). The as-synthesized materials appear to be quite homogeneous, despite their high vanadium content, as evidenced by their amorphous PXRD diffractograms after calcination at 300 °C in O₂.

The variation in both silicon content and vanadium oxidation state in **1**, **2**, and OV[OSi(O^tBu)₃]₃ allows a comparison of how these features alter the physical properties of materials that are generated via the thermolytic molecular precursor route. In general, for these V/Si/O materials, higher silicon content in the precursor yields a material with a higher surface area. However, a higher silicon content appears to drive the formation of larger V₂O₅ crystallites earlier in the calcination process. The oxidation state of the vanadium in the molecular precursor appears to also dramatically influence the nature of the ultimate material, with the V(IV) precursors giving rise to as-synthesized materials that are more homogeneous than those synthesized using the V(V) precursor. As expected, the precursors with the highest vanadium content produce the most

V₂O₅ (in the form of small crystallites) after calcination at 500 °C. These results suggest that the best single-source molecular precursors for well-dispersed V/Si/O materials will feature vanadium in a low oxidation state.

Despite their inherent phase separations at elevated temperatures, the materials derived from **1** and **2** should be well-suited as heterogeneous catalysts for reactions that occur at temperatures below 400 °C, with the materials derived from **2** being perhaps the best candidates due to their higher surface areas. Co-thermolyses of **1** or **2** with alkoxides (e.g., Zr(OR)₄, [Al(OR)₃]_n, etc.) should prove effective for the formation of high surface area oxidation catalysts featuring zirconia or alumina supports.^{14,19} In addition, the grafting of complexes **1** and **2** onto support materials may allow for the preparation of catalytic materials with site-isolated vanadium centers.¹⁸

Experimental Section

General. All synthetic manipulations were performed under an atmosphere of nitrogen using standard Schlenk techniques and/or a vacuum atmospheres drybox, unless noted otherwise. All solvents used were distilled from sodium/benzophenone, potassium/benzophenone, sodium, or calcium hydride, as appropriate. The ¹H NMR spectra were recorded using a Bruker AMX300 (at 300 MHz) spectrometer. Benzene-d₆, vacuum-transferred from a Na/K alloy, was used as the solvent for all NMR studies. Infrared spectra were recorded using a Mattson Infinity Series FTIR spectrometer with all samples being pressed into KBr disks. Electronic absorption spectra were recorded using a Hewlett-Packard 8452A diode array spectrophotometer with all samples loaded into a quartz cuvette (1-cm path length, equipped with a PTFE valve) as *n*-octane solutions under a nitrogen atmosphere in a drybox. Electron paramagnetic resonance spectra were recorded using a Bruker EMX spectrometer operating in the X band mode. Spectra were collected on samples in *n*-octane solution at room temperature. Thermal analyses were performed using a TA Instruments SDT 2960 integrated thermogravimetric/differential scanning calorimetric analyzer (TGA/DSC). Surface area and pore volume analyses were performed using a Quantachrome Autosorb 1 surface area analyzer with all samples heated at 120 °C, under vacuum, for a minimum of 4 h immediately prior to data collection. X-ray powder diffraction data were obtained using a Siemens D5000 diffractometer operating with θ -2 θ geometry at room temperature. The PXRD data were collected using Cu K α radiation (λ = 1.5406 Å), a collection time of 1.5 s, and a step size of 0.02°. Transmission electron microscopic images were obtained using a JEOL 200cx transmission electron microscope at an operating accelerating voltage of 200 kV. Samples for TEM analyses were prepared via deposition using a hexane suspension of finely ground material on a "Type A" carbon-coated copper grid obtained from Ted Pella Inc. Elemental analyses of **1** and **2** were performed by the College of Chemistry Micro-Mass Facility at the University of California, Berkeley. Analyses for Si and V were performed by Desert Analytics, Tucson, AZ. V(O^tBu)₄⁴³ and HOSi(O^tBu)₃⁴⁴ were prepared by literature procedures.

(tBuO)₃VOSi(O^tBu)₃ (1**).** Toluene (5 mL) was added to a mixture of V(O^tBu)₄ (1.439 g, 4.19 mmol) and HOSi(O^tBu)₃ (1.108 g, 4.19 mmol) in a Schlenk tube under flowing N₂. The tube was heated to 80 °C and the reaction mixture was magnetically stirred for 24 h. The volatiles were removed in vacuo at room temperature, leaving a light blue solid residue. The residue was taken up in toluene (6 mL) and acetonitrile was subsequently added (2 mL). The resulting solution was stored at -30 °C for 24 h, yielding a light blue crystalline material that was contaminated with a small amount of HOSi-

(43) Bradley, D. C.; Mehta, M. L. *Can. J. Chem.* **1962**, *40*, 1183.

(44) Abe, Y.; Kijima, I. *Bull. Chem. Soc. Jpn.* **1969**, *42*, 1118.

(*O*Bu)₃. Washing with acetonitrile (5 mL) and recrystallization of this material from a 3:1 toluene/acetonitrile mixture at -30 °C produced analytically pure light blue platelike crystals of **1** in moderate yield (1.006 g, 1.88 mmol, 45%). Anal. Calcd for C₂₄H₅₄O₇SiV (%): C, 54.01; H, 10.20. Found: C, 53.80; H, 10.10. IR (cm⁻¹): 2975 s, 2932 w, 2902 vw, 2876 vw, 1473 w, 1390 m, 1366 s, 1244 m, 1194 s, 1063 vs, 1028 m, 1012 m, 941 m br, 924 m sh, 908 m sh, 829 w, 791 w, 701 m, 613 w br, 513 vw, 479 vw, 430 vw. ¹H NMR (benzene-*d*₆, 300 MHz): δ 3.5 (s vbr, 27 H, V(*O*^tBu)₃), 1.5 (s br, 27 H, Si(*O*^tBu)₃). EPR: *g*-factor = 1.974(3); *A* = 70(1). UV-vis: 248 nm (ε = 2278), 296 nm (ε = 2308), 322 nm (ε = 2237), and 740 nm (ε = 203).

(BuO)₂V[OSi(*O*Bu)₃]₂ (2). A toluene (5 mL) solution of HOSi(*O*Bu)₃ (1.035 g, 3.91 mmol) was added to a toluene (5 mL) solution of V(*O*Bu)₄ (0.672 g, 1.96 mmol) in a Schlenk tube under flowing N₂. The tube was heated to 80 °C and the reaction mixture was magnetically stirred for 24 h. Subsequent cooling to room temperature and removal of the volatiles in vacuo left a dark blue viscous liquid. The resulting liquid was then heated to 80 °C under reduced pressure for a brief time (10–15 min) to remove unreacted HOSi(*O*Bu)₃ (small amounts). The remaining viscous liquid was taken up in toluene (6 mL), acetonitrile (2 mL) was added, and the solution was stored at -30 °C for 24 h. Analytically pure bright blue needlelike crystals were obtained from two crops (each washed with 5 mL of acetonitrile). The total amount of pure material isolated was 0.861 g (1.19 mmol, 61%). Anal. Calcd for C₃₂H₇₂O₁₀Si₂V (%): C, 53.08; H, 10.02. Found: C, 52.99; H, 10.01. IR (cm⁻¹): 2976 vs, 2931 m, 2907 w, 2874 vw, 1473 vw, 1459 vw, 1389 m, 1364 s, 1241 s, 1194 s, 1062 vs, 1028 s, 944 vs br, 922 vs sh, 909 vs sh, 831 m, 791 w, 702 m, 637 vw, 607 vw, 512 vw, 497 w, 475 m, 430 vw. ¹H NMR (benzene-*d*₆, 300 MHz): δ 4.5 (s vbr, 18 H, V(*O*^tBu)₂), 1.5 (s br, 54 H, Si(*O*^tBu)₃). EPR: *g*-factor = 1.973(4); *A* = 72(3). UV-vis: 250 nm (ε = 3062), 296 nm (ε = 2828), and 765 nm (ε = 173).

It should be noted that attempted syntheses of (BuO)V[OSi(*O*Bu)₃]₃ and V[OSi(*O*Bu)₃]₄ via silanolysis reactions were unsuccessful.

VOSi_{1ss} and VOSi_{2ss}. Representative solid-state thermolyses were carried out as follows: A sample of either **1** (0.162 g, 0.304 mmol) or **2** (0.286 g, 0.395 mmol) was added to a thick-walled Pyrex pyrolysis tube in a glovebox (N₂ atmosphere). The tube was then evacuated for 1 h and sealed with a torch. The tube was placed in a preheated oven at 180 °C for 18 h, cooled to room temperature, and opened in the air. The brown solid that remained was then transferred to a Schlenk tube, dried for 2 h in vacuo, and stored under N₂. The mass of each product was as follows: **VOSi_{1ss}**, 0.042 g (25.9% ceramic yield); **VOSi_{2ss}**, 0.096 g (33.6% ceramic yield). Calcinations were carried out in a Lindberg 1200 °C three-zone tube furnace in an O₂ atmosphere (100 mL min⁻¹). The heating rate was 10 °C min⁻¹ and the final temperature was maintained for 2 h.

VOSi_{1xg} and VOSi_{2xg}. Representative solution thermolyses were carried out as follows: A thick-walled Pyrex pyrolysis tube was charged with an *n*-octane (5.0 mL) solution of either **1** (0.251 g, 0.470 mmol) or **2** (0.362 g, 0.500 mmol) in a glovebox (N₂ atmosphere). The tube was flame-sealed after three freeze-pump-thaw cycles and placed in a preheated oven at 180 °C for 24 h. A dark brown gelatinous precipitate was observed in all cases after the 24-h heating period. The tube was cooled to room temperature and opened in the air. The gel was air-dried for 1 day and subsequently dried in vacuo for 2 h and stored under N₂. The mass of each xerogel product was as follows: **VOSi_{1xg}**, 0.077 g (30.7% ceramic yield); **VOSi_{2xg}**, 0.099 g (27.3% ceramic yield). Calcinations of the xerogels were carried out in a Lindberg 1200 °C three-zone tube furnace in O₂ (100 mL min⁻¹). The heating rate was 10 °C min⁻¹ and the final temperature was maintained for 2 h.

NMR Study of the Solution Thermolyses of 1 and 2. Representative thermolyses were carried out as follows: compound **1** (18.5 mg, 0.0347 mmol) and ferrocene (11.3 mg, 0.0607 mmol) were dissolved in benzene-*d*₆ and sealed in an NMR tube after three freeze-pump-thaw cycles. The tube was heated in an oil bath at 180 °C for 1 h, until decomposition

was evident. The identifiable, soluble decomposition products were quantified by integration against the ferrocene standard: CH₂=CMe₂ (0.153 mmol); HOSi(*O*Bu)₃ (0.011 mmol); ^tBuOH (trace); H₂O (trace). Compound **2** (19.2 mg, 0.0265 mmol) and ferrocene (12.2 mg, 0.0656 mmol) were treated similarly to give the following identifiable soluble products: CH₂=CMe₂ (0.161 mmol); HOSi(*O*Bu)₃ (0.014 mmol); ^tBuOH (0.004 mmol); H₂O (trace). In all cases, overlapping resonances were observed at 0.86 and 0.84 ppm, attributable to soluble species likely containing ^tBu groups. We were unable to determine the identities of these species (by GC-MS analysis); however, the small amount of each (the total integration for both was ca. 0.5 times the integration for the HOSi(*O*Bu)₃ resonance) renders these insignificant in the context of the studies described here.

Structure Determinations for 1 and 2. Crystals of **1** and **2** were mounted on quartz fibers using Paratone N hydrocarbon oil. All measurements were made on a SMART CCD area detector with graphite monochromated Mo Kα radiation. Cell constants and an orientation matrix were obtained from a least-squares refinement using the measured positions of 741 reflections (*I* > 10σ(*I*)) in the range 3.00 < 2θ < 41.1° for **1** and 3011 reflections (*I* > 10σ(*I*)) in the range 3.00° < 2θ < 46.8° for **2**. Data were integrated using the program SAINT (SAX Area-Detector Integration Program, V5.04; Siemens Industrial Automation, Inc.: Madison, WI, 1995) to a maximum 2θ value of 41.1° for **1** and 46.8° for **2**. The data were corrected for Lorentz and polarization effects. An empirical absorption correction based upon a comparison of redundant and equivalent reflections was applied using SADABS (Siemens Area Detector Absorption Corrections; Sheldrick, G. M., 1996) (*T*_{max} = 0.98, *T*_{min} = 0.53 for **1**; *T*_{max} = 0.98, *T*_{min} = 0.74 for **2**). The structures were solved by direct methods and expanded using Fourier techniques with all calculations performed using the SHELXTL crystallographic software package (Sheldrick, G. M. Siemens SHELXTL, V5.03; Siemens Crystallographic Research Systems: Madison, WI, 1994). The disorder in the V and Si positions for **1** was modeled such that the occupancies of V1, Si1, V2, and Si2 were all 50%, with V# and Si# having the same *x*, *y*, and *z* coordinates. Refinement with the occupancies of these atoms as free variables also suggested a 50:50 disorder model. The non-hydrogen atoms of **1** and **2** were refined anisotropically. Hydrogen atoms were included in calculated idealized positions but not refined. The final cycle of full-matrix least-squares refinement (using *F*²) for **1** was based upon 1347 observations (*I* > 2σ(*I*)) and 298 variable parameters. The final cycle of full-matrix least-squares refinement (using *F*²) for **2** was based upon 3342 observations (*I* > 2σ(*I*)) and 406 variable parameters. The maximum and minimum peaks in the final difference maps were 0.37 and -0.28 e⁻ Å⁻³ for **1** and 0.637 and -0.367 e⁻ Å⁻³ for **2**.

Acknowledgment. This work was supported by the Director, Office of Energy Research, Office of Basic Energy Sciences, Chemical Sciences Division, of the U. S. Department of Energy under Contract DE-AC03-76SF00098. We thank Professors A. Stacy (PXRD) and A. Bell (Raman) for the use of instrumentation.

Supporting Information Available: Tables of crystal, data collection, and refinement parameters, bond distances and angles, and anisotropic displacement parameters for **1** and **2** (PDF and CIF). This material is available free of charge via the Internet at <http://pubs.acs.org>.

CM011524G